Journal of Thermal Analysis and Calorimetry, Vol. 63 (2001) 21–30

THERMAL GRADIENTS IN TMDSC SAMPLES
A comparison of theory and experimental data

F. U. Buehler and J. C. Seferis[*]

Polymeric Composites Laboratory, University of Washington, Seattle, WA 98195, USA

(Received June 4, 2000)

Abstract

Until recently, the issue of the thermal gradients within TMDSC samples remained mostly a subject of theory and mathematical models – only the phase lag was subject to experimental verification, as this information is readily available from the analysis software of most instruments. There was no method to verify the transient behaviour and temperature gradients within a sample without making costly and intensive modifications to the equipment. Recently, however, a group of researchers were able to experimentally measure thermal profiles as a function of sample thickness with a high-speed, high-resolution infrared camera mounted on the TMDSC cell. Therefore, this paper is dedicated to comparing the predictions of our three-dimensional model with this newly available data.

Keywords: infrared thermography, modeling, phase lag, sample thickness, thermal gradients, TMDSC

Introduction

TMDSC theory was discussed at length previously [1–3], and will not be repeated here. Instead, this section puts emphasis on the configuration of the actual TMDSC instrument.

In a standard instrument, a heater controls the block (furnace) temperature. As the sample rests on the block, the bottom temperature of the sample can be assumed to be equal to that of the block. Below the block sits a temperature sensor, the signal from which is considered by the instrument as the sample temperature. A graphical representation of the set-up is shown in Fig. 1.

Four temperature gradients pertain in the TMDSC cell. These are found (1) between the heater and the temperature sensor, (2) between the sensor and the block, (3) between the block and the bottom of the sample, and (4) between the bottom and top of the sample. For all practical purposes, T_{block} can be assumed equal to T_{bottom}, since the wall of the aluminum pan is very thin (~0.08 mm).

Gradients (1) and (2) do not depend on the sample, but on the instrument configuration. On the TMDSC market, two types of instruments are found: power compen-

* Author to whom all correspondence should be addressed.

1418–2874/2001/ $ 5.00

Akadémiai Kiadó, Budapest
Kluwer Academic Publishers, Dordrecht

sated and heat flux. Both types achieve the same results in terms of thermal analysis: they only differ in their design. Power compensated calorimeters have two individual heaters, one under the sample, one under the reference. According to this design, both specimens are kept at the same temperature by controlling the power input to these heaters. Therefore, the output signal is an electrical power. In the second design, the heat flux calorimeter, only one heater is present, and it heats both specimens (sample and reference). Due to their different thermophysical properties, reference and sample will have different temperatures. This temperature difference is measured by thermocouples, and it is the output signal for the heat flux calorimeters. Besides the differences in design, each instrument maker can have various control systems, which make each model unique.

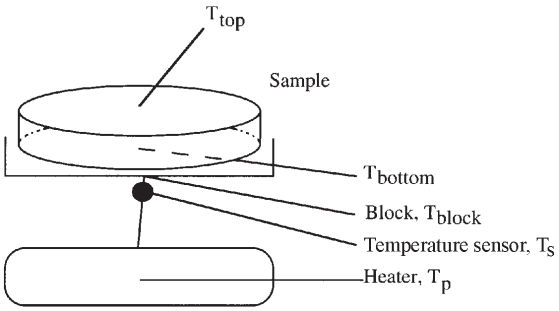

Fig. 1 Typical configuration of a TMDSC cell

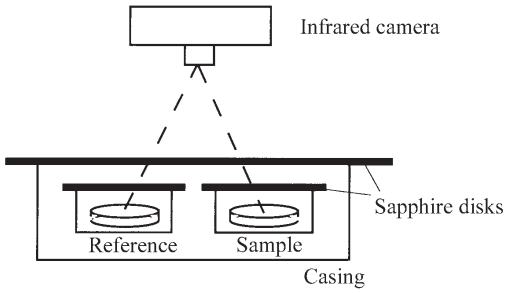

Fig. 2 Schematic of the camera set-up over the DSC cell

Experimental

Calorimeter and specimen set-up

Androsch *et al*. used a power-compensated Perkin Elmer DSC 7 for their data collection [4]. The commercial instrument was modified to allow infrared measurement of the various temperature gradients, as illustrated in Fig. 2. Each furnace was covered with small sapphire disks instead of the original metallic lids. Sapphire was chosen as it is transparent in the 3–5 μm wavelength infrared region, while limiting heat losses

to the environment. For the same reasons, the calorimeter casing lid was replaced with a large sapphire disc. Mounted on top of the calorimeter, an infrared camera allowed direct non-contact measurement of the temperature.

Experimental parameters

To measure top and bottom sample temperatures, Androsch *et al*. used an open, half-filled sample, as depicted in Fig. 3 [4]. All experiments were conducted quasi-isothermally at 423 K with saw-tooth type modulation of 0.5, 1.0, 2.0, 4 and 20, 30, 40 and 60 s periods, respectively [4].

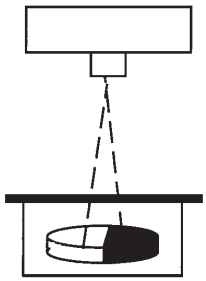

Fig. 3 Half-filled, open pan was used to determine top and bottom temperatures

The temperature amplitude as measured by the infrared camera was denoted as A_{IR}, while the amplitude measured by the temperature sensor was designated A_{Ts}. These two amplitudes, A_{IR} and A_{Ts}, were compared to the programmed amplitude A_{Tp}, by calculating the following dimensionless normalized differences D_{IR} and D_{Ts} [4]:

$$D_{IR} = \frac{A_{Tp} - A_{IR}}{A_{Tp}} \tag{1a}$$

$$D_{Ts} = \frac{A_{Tp} - A_{Ts}}{A_{Tp}} \tag{1b}$$

A_{Tp} corresponds to the temperature amplitude that the user entered, which was considered to be equal to the heater temperature. A_{Ts} was given by the instrument as being the sample temperature, but was actually the temperature measured by the sensor, which was shown by Androsch *et al*. to be equal to the furnace temperature [4]. A_{IR}, which can be either $A_{IRbottom}$ or A_{IRtop}, corresponds to the actual, measured temperature of the bottom or top of the sample, respectively, as determined by infrared analysis [5].

Samples

Androsch *et al*. performed their experiments on commercial poly(ethylene terephthalate) (PET) film, molten poly(ethylene-co-octane) (PEO), and poly(butylene terephthalate) (PBT) [4]. PET samples were prepared in five different thicknesses by stacking layers of

a 0.1 mm film in the DSC pans. PEO samples, which were completely melted at the testing temperature of 423 K, were prepared in two thicknesses only, and the PBT samples were investigated only for one single thickness. As a result, the present article focused on the PET samples, for which more data were generated and for which more elaborate investigations were provided by Androsch *et al.* in their paper [4].

Infrared camera

In their work, Androsch *et al*. used a high-speed, high sensitivity, high-resolution infrared camera, the details of which are available in their article [4]. Snapshots of the sample temperature profile were taken at 0.5 s intervals, with an integration time of about 1 ms. Resolution on 256×256 pixel surface was about 0.2–0.5 mm per pixel, depending on the camera position away from the samples. Samples subjected to infrared measurements were sprayed with graphite or black paint to minimize emission of radiation.

Results and discussion

Thermal gradient between sample top and bottom surfaces

For PET samples of various thickness, the deviation between programmed and measured temperature amplitude as a function of modulation period for sample's top and bottom surfaces is shown in Fig. 4. Similarly, the influence of sample thickness is summarized in Fig. 5. Four observations were derived from these figures.

First, the sample bottom temperature amplitude and programmed temperature amplitude were not equal (i.e. $D_{\mathrm{IRbottom}}\neq 0$). This was explained by the existence of a thermal resistance between heater and sample: the bottom of the sample was separated from the heater by an aluminum layer (the bottom of the DSC pan), the block (on which the pan rested), and the temperature sensor. This resistance to heat transfer is also at the origin of the instrumental phase lag, which was experimentally observed earlier [2].

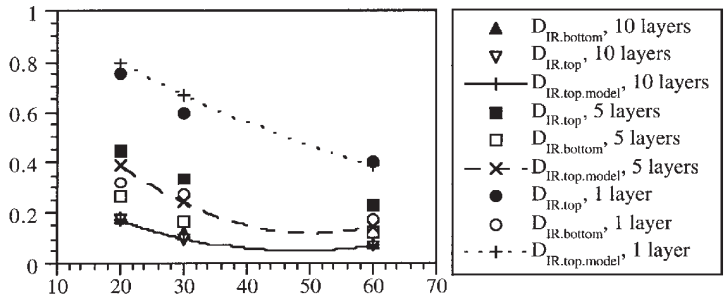

Fig. 4 Deviation between programmed and measured modulation amplitude as given by Eq. (1) for PET samples. Uncovered samples with A_{Ts}=1 K. Shown are 1, 5, and 10 layer thick samples. Dashed lines are proposed model with $\alpha=4.9\cdot10^{-8}$ m^2 s^{-1}

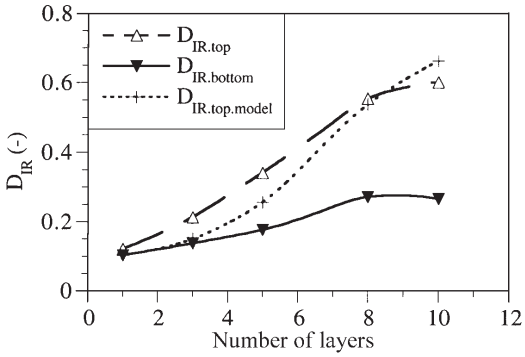

Fig. 5 Deviation between programmed and measured modulation amplitude as given by Eq. (1) for PET samples. Uncovered samples with period of 30 s and amplitude of 0.5, 1, 2, and 4 K. Dashed lines is proposed model with $\alpha=5.0\cdot10^{-8}$ m^2 s^{-1}

Second, the temperature amplitude at the top of the sample decreased as sample thickness increased (D_{IRtop} increased as the number of PET layers increased in the DSC pan). This means that the diffusion of heat through the sample was affected by the length of the diffusion path. Therefore thicker samples were experiencing more dampening of the temperature amplitude, hence the lower amplitude at their top surface.

Third, both top and bottom sample temperature amplitude increased as the period increased ($D_{\mathrm{IRtop,bottom}}$ decreased as period increased, Fig. 4). The temperature amplitude dampening being directly proportional to the heating rate, long periods provided more time for the temperature profile to develop. This yielded higher temperature amplitudes at the top surface of the samples for greater periods.

Fourth, the programmed temperature amplitude did not affect the deviation between programmed and measured temperature amplitudes (D_{IR} was not affected by changes in A_{Tp}). Although not visible on Fig. 5, the original figure by Androsch *et al*. displayed data for four different programmed temperature amplitudes, which coincided so closely in their respective D_{IR} that only one data point could be represented for each four in Fig. 5 [4]. To understand this observation, one has to refer back to Eqs (42), (43) and (46) of [1] from which it can be demonstrated that:

$$A_{\mathrm{IR}} = A_{\mathrm{Tp}} \sqrt{\left(1-\omega R^2 \frac{1}{\Lambda_i'}\right)^2 + \left(\omega R^2 \frac{1}{\Lambda_i''}\right)^2} \tag{2}$$

From Eqs (1) and (2), the deviation between programmed and measured temperature amplitudes becomes:

$$D_{\mathrm{IR}} = 1-\sqrt{\left(1-\omega R^2 \frac{1}{\Lambda_i'}\right)^2 + \left(\omega R^2 \frac{1}{\Lambda_i''}\right)^2} \tag{3}$$

hence D_{IR} does not depend on A_{Tp}.

On Fig. 4, the proposed model was found to represent the experimental data satisfactorily for low and high thickness samples, but did poorly at intermediate thickness. Similar findings were observed on Fig. 5. Note that Androsch *et al*. suggested a linear dependence between D_{IR} and thickness, which was not found by the present model. Comparison between models and experimental data is provided below, after discussion of the phase lag data.

Phase lag between sample top and bottom surfaces

Figure 6 shows the influence of sample thickness on the phase lag φ between the top and bottom surfaces of a PET sample. First, the phase lag was not found to depend on the programmed temperature amplitude A_{Tp}. This was expected by the present model through Eq. (20) of [3] and is a direct consequence of the fact that D_{IR} did not depend on A_{Tp}, as observed in the previous paragraph. Second, the phase lag was found to increase with sample thickness. Thick samples having a longer path of diffusion for heat, the phase lag between top and bottom surfaces was anticipated to be greater for thicker samples. From Fig. 6, it can be seen that the proposed model corroborated the phase lag data collected by Androsch *et al*. over the entire range of studied thicknesses. The most adequate fit was obtained for $\alpha=7.9\cdot10^{-8}$ m^2 s^{-1}.

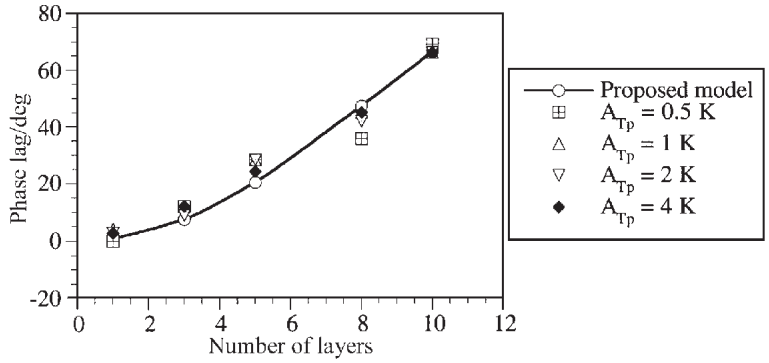

Fig. 6 Phase lag between top and bottom surfaces of PET samples of various thickness for a series of programmed temperature amplitudes. Model curve with $\alpha=7.9\cdot10^{-8}$ m^2 s^{-1}

Comparison between models

In their works, Androsch *et al.* proposed a one-dimensional model for TMDSC. These authors assumed that the sample was a semi-infinite solid, with heat introduced through its bottom surface. According to Gröber and Erk, the decrease of the temperature amplitude as a function of x, the distance from the bottom surface, is [6]:

$$A(x)=A(0)\exp\left(-x\sqrt{\frac{\pi}{\alpha p}}\right) \tag{4}$$

where $A(x)$ and $A(0)$ are the temperature amplitudes at a distance x from the surface and at the surface of the sample, respectively; α is the sample thermal diffusivity; and p the period of modulation. Similarly, the phase angle φ at position x is given by [6]:

$$\varphi = 180x\sqrt{\frac{1}{\alpha p \pi}} \tag{5}$$

Figure 7 is a comparative plot between the ratio $A(x)/A(0)$, as calculated by the present model and by the model considered by Androsch *et al*. None of the models was found to describe precisely the experimental data over its entire range. The model suggested by Androsch *et al*. underestimated $A(x)$, especially in the case of

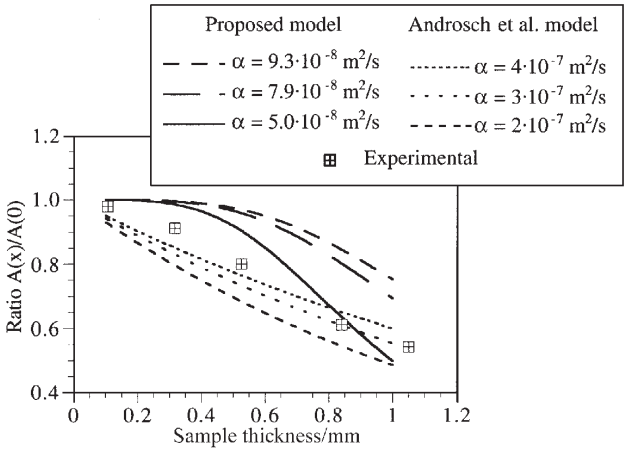

Fig. 7 Normalized decrease of modulation amplitude *vs*. sample thickness, experimental data and fit by the model developed in this work and by that of Androsch *et al*.

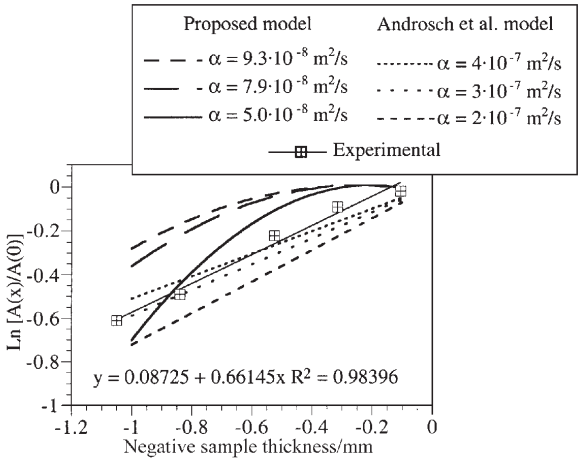

Fig. 8 Same as Fig. 7, but linearized

thin samples. Conversely, the model developed in this work did the opposite, i.e. it overestimated $A(x)$ in thin samples. Androsch *et al*. considered the sample as a uni-dimensional and semi-infinite solid. Therefore, their model was expected to perform poorly for thin samples, and to gradually improve as sample thickness increased. This prediction was observed in Fig. 7, where it was found that a thermal diffusivity of $3 \cdot 10^{-7}$ m^2 s^{-1} described satisfactorily samples of thickness 0.5 mm and greater. Additionally, the Androsch model predicted the logarithm of the normalized decrease of modulation amplitude, $\ln[A(x)/A(0)]$, to be proportional to the negative of the sample thickness, $(-x)$. Such a dependence was observed in the experimental data, as shown in Fig. 8, with a coefficient of regression R^2 of 0.98396. Unfortunately for Androsch *et al.*, the value of thermal diffusivity that provided their best fit was three times as much as that found in literature, as seen in Fig. 9. The present model did not

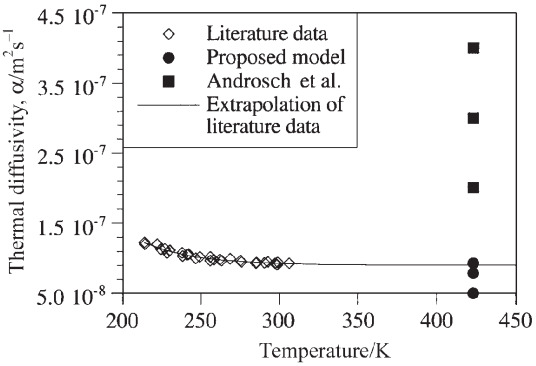

Fig. 9 Literature values for the thermal diffusivity of PET [7, 9] and best-fitted values as obtained from mathematical models

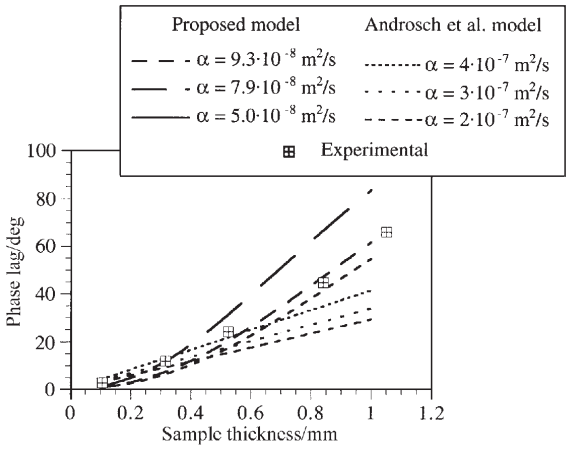

Fig. 10 Phase lag of modulation between top and bottom of the PET sample as function of sample thickness, experimental data and fit by the model developed in this work and by that of Androsch *et al*.

succeed to describe the temperature amplitude data, overestimating the latter over the entire thickness range. The origin of this discrepancy was sought in the hypothesis made for the model, which included a cylindrically shaped sample. As Androsch *et al*. used a half-sample to enable their temperature measurements, this did not fulfil the hypothesis anymore. It is therefore difficult to discuss the present model without making major modifications to the assumptions that are at the base of the model, and consequently without completely re-deriving the equations.

In addition to temperature amplitude, both models were tested for their predictability in terms of phase lag. Figure 10 shows phase lag between top and bottom as measured experimentally, and as calculated by both models. It was found that the proposed model gave very good results over the entire PET sample thickness range. Moreover, the best fitting thermal diffusivity was of about $7.9 \cdot 10^{-8}$ m^2 s^{-1}, which is very close to the literature value at 306 K which is about $9.3 \cdot 10^{-8}$ m^2 s^{-1} [7]. As observed in Fig. 10, Androsch's model underestimated the phase lag φ for thicker samples. Due to the semi-infinite sample hypothesis, that model was expected to perform best for thick samples, which was not observed.

Conclusions

For the first time, direct measurements of the temperature gradients inside a PET sample subject to TMDSC conditions were realized by a research group that used a high-speed, high-sensitivity infrared camera. Their experimental results were compared to two mathematical models of heat diffusion. The first model, which was introduced in earlier publications [1–3], provided a very accurate representation of the phase lag for thin as well as thick samples. Part of the model parameters, the thermal diffusivity used for the computations was in good agreement with that of literature. This first model did however perform poorly in the description of the thermal gradients observed along the axial direction of the sample. This poor performance was attributed to geometry differences between the actual sample and the modelled sample. The second model, proposed by Androsch *et al.*, showed superior performance in the description of the sample axial temperature gradient, especially in the case of thick samples. It did however not represent the sample phase lag satisfactorily, and based its calculations on a thermal diffusivity that appeared excessively large.

* * *

The authors express their appreciation to Prof. B. Wunderlich and co-workers for sharing their latest results in a timely manner. Support for this work was provided by The Boeing Company through the Boeing-Steiner professorship.

Nomenclature

Latin letters

A/K	amplitude of the temperature modulation
D/–	normalized difference in temperature amplitude

R/m	radius of the specimen
P/s	period of modulation
X/m	distance from the bottom surface of the specimen

Indic es

IR	measured by infrared analysis
block	block (furnace) of the calorimeter
bottom	bottom surface of the specimen
p	user programmed
s	sensor
top	top surface of the specimen

Greek letters

Λ'/m^2 s^{-1}	effective thermal diffusivity term that arises in the in-phase component of the specimen temperature
Λ''/m^2 s^{-1}	effective thermal diffusivity term that arises in the out-of-phase component of the specimen temperature
α/m^2 s^{-1}	thermal diffusivity
φ/rad	phase angle between sample's top and bottom surface temperature
ω/rad s^{-1}	pulsation of the modulation

References

1 F. U. Buehler, C. J. Martin and J. C. Seferis, J. Therm. Anal. Cal., 54 (1998) 501.
2 F. U. Buehler and J. C. Seferis, Thermochim. Acta, 334 (1999) 49.
3 F. U. Buehler and J. C. Seferis, Thermochim. Acta, 348 (2000) 161.
4 R. Androsch, M. Pyda, H. Wang and B. Wunderlich, J. Therm. Anal. Cal., 61 (2000) 661.
5 H. Wang, M. Bartkowiak, F. A. Modine, R. B. Dinwiddie, L. A. Boatner and G. D. Mahan, J. American Ceramic Soc., 81 (1998) 2013.
6 H. Gröber and S. Erk, Fundamentals of Heat Transfer, McGraw-Hill, New York 1961.
7 J. Brandrup and E. H. Immergut, Polymer Handbook, Wiley, New York 1989.
8 Y. S. Touloukian, R. W. Powell, C. Y. Ho and M. C. Nicolaou, Thermophysical Properties of Matter Touloukian, Y. S., Ed. IFI/Penum, New York 1973.